JOURNAL OF COMPUTATIONAL PHYSICS 115, 288–295 (1994)

Finite Element Solutions to *GaAs–AlAs* Quantum Wells with Connection Matrices at Heterojunctions

TSUNG L. LI AND KELIN J. KUHN

Department of Electrical Engineering, FT-10, University of Washington, Seattle, Washington 98195

Received January 18, 1994; revised April 28, 1994

In this paper, the irreducible finite element formulations for the solutions to the single-band effective-mass equation are developed to incorporate the connection conditions at the heterojunctions. The exact interface formulation utilizes the exact form of the connection matrix. The finite-difference interface formulation uses the finite difference approximation to the connection matrix. For the investigation of the *GaAs–AlAs* quantum well, the finite-difference interface formulation has to be employed, and the relative errors are shown to be less than 10^{-3}. Then, this finite element formulation is utilized to compare the effects of the electric field on the *GaAs–AlAs* quantum well with the heterojunctions modeled by the conventional, the effective-mass-dependent, and the energy-dependent connection matrices. It is found that the eigenenergies predicted by the models with non-conventional connection matrices are larger in magnitude and less dependent on the electric field than the conventional model.

1. INTRODUCTION

The effective-mass equation is valid for a semiconductor with a gradually varying potential [1]. However, it is known that the abruptness of a heterojunction does not fulfill this requirement. Many researchers have dealt with this difficulty by introducing the connection matrix ($\tilde{\mathbf{T}}_{BA}$) for the envelope function ($\tilde{\psi}$) and its derivative at the heterojunction [2–7],

$$\begin{bmatrix} \tilde{\psi}^B(\tilde{z}_n) \\ \nabla\tilde{\psi}^B(\tilde{z}_n) \end{bmatrix} = \tilde{\mathbf{T}}_{BA} \begin{bmatrix} \tilde{\psi}^A(\tilde{z}_n) \\ \nabla\tilde{\psi}^A(\tilde{z}_n) \end{bmatrix}, \tag{1}$$

with

$$\tilde{\mathbf{T}}_{BA} = \begin{bmatrix} t_{11} & t_{12} \\ t_{21} & t_{22} \end{bmatrix},$$

where $\tilde{\psi}^A$ and $\tilde{\psi}^B$ are the envelope functions in materials A and B, respectively, and $\tilde{z}_n$ is the location of the interface. Material A is the first-grown material and will be drawn on the left-hand side of the heterojunction ($\tilde{z} < \tilde{z}_n$), while material B will be on the right-hand side ($\tilde{z} > \tilde{z}_n$). $\tilde{\mathbf{T}}_{BA}$ is the 2×2 connection matrix, and t_{11}, t_{12}, t_{21}, and t_{22} are its matrix elements. $\nabla = a \cdot d/d\tilde{z}$ with a being the lattice constant.

In the absence of the external field, the single-band effective-mass equation incorporated with connection matrices at heterojunctions can be solved analytically by the transfer matrix method [8]. However, for the investigation of the field effects, numerical methods become important.

The finite element formulation incorporating the connection matrix was first published by K. Nakamura *et al.* to investigate quantum wells [9, 10] and superlattices [11, 12]. They also applied their numerical techniques to the computation of the optical properties of quantum wells [13] and to resonant tunneling through a potential barrier [14]. In their work, the numerical analysis is a mixed formulation, in which the envelope function and its first derivative are treated as unknowns at each node [15]. The shape functions they used are third-order Hermitian line elements.

This paper presents two irreducible finite element formulations, where only the envelope function is regarded as unknown at each nodal point. The exact interface formulation is valid only if $t_{12} \neq 0$. The finite-difference interface formulation holds for any value of t_{12}. The advantages of this approach are (1) that, for the same number of nodes, it requires about a half of the memory used by the mixed formulation if the shape functions of the same order are employed, and (2) that simple first-order shape functions can be employed. The disadvantage of this approach is that, at least for the *GaAs–AlAs* quantum well, the finite-difference interface formulation has to be utilized because $t_{12} = 0$, and the finite-difference interface formulation is not as accurate as the exact interface formulation.

In this paper, the accuracy of the finite-difference interface formulation is investigated by using the rectangular *GaAs–AlAs* quantum well as an example. The accuracy of the finite-difference interface formulation is found to be satisfactory (the relative error being less than 10^{-3}). Then, this finite element formulation will be used to compare the electric field effects on the *GaAs–AlAs* quantum well predicted by three types of connection matrices found in the literature. The three types of connection matrices are called the conventional, the effective-mass-dependent, and the energy-dependent connection matrices in

0021-9991/94 $6.00

this paper. The conventional connection matrix is the matrix form of the conventional interface conditions of the continuity of the envelope function and the probability flux based on the envelope function [16]. The effective-mass-dependent connection matrix is the connection matrix obtained from the tight-binding model by T. Ando *et al.* [5]. The energy-dependent connection matrix is the connection matrix calculated from the pseudopotential model by J. P. Cuypers *et al.* [7].

2. FINITE ELEMENT FORMULATIONS

In this paper, the physical quantities with the units of mass, length, and energy are normalized by the electron rest mass (m_0), the characteristic length (L), and the characteristic energy (V_0) of the system, respectively. The envelope function is normalized by $1/\sqrt{L}$. The single-band effective mass equation [17] and the interface connection conditions [5, 7] at the heterojunctions become

$$-\frac{\kappa^2}{2}\frac{d}{dz}\left[\frac{1}{m(z)}\frac{d\psi(z)}{dz}\right] + V(z)\psi(z) = E\psi(z) \tag{3}$$

with

$$\kappa = \frac{\hbar}{\sqrt{m_0 V_0 L^2}}, \tag{4}$$

and

$$\begin{bmatrix} \psi^B(z_n) \\ d\psi^B(z_n)/dz \end{bmatrix} = \begin{bmatrix} t_{11} & t_{12}(a/L) \\ t_{21}(L/a) & t_{22} \end{bmatrix} \begin{bmatrix} \psi^A(z_n) \\ d\psi^A(z_n)/dz \end{bmatrix}, \tag{5}$$

where z, $m(z)$, $V(z)$, $\psi(z)$, and E are the normalized representations of the location, the effective mass, the potential, the envelope function, and the eigenenergy, respectively. $2\pi\hbar$ is the Planck's constant, and z_n is the location of the heterojunction. The quantities with superscripts of A and B mean the functional values evaluated in materials A and B, respectively. a is the lattice constant. t_{11}, t_{12}, t_{21}, and t_{22} are the matrix elements of the connection matrix given by Eq. (2).

The truncated boundary conditions used are

$$\psi(x_1) = \psi(x_2) = 0, \tag{6}$$

where the envelope function becomes sufficiently small at x_1 and x_2.

For simplicity, the notation employed in the rest of this section is

$$\alpha(z) = \frac{\kappa^2}{2}\frac{1}{m(z)}, \tag{7}$$

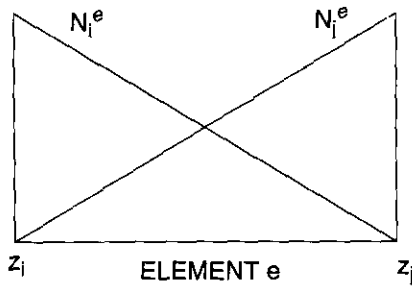

FIG. 1. The linear shape functions. The first-order shape functions employed in this paper are $N_i^e = 1 - \eta$ and $N_j^e = \eta$ for the eth element, where $\eta = (z - z_i)/(z_j - z_i)$.

$$\beta(z) = V(z), \tag{8}$$

and

$$\lambda = E. \tag{9}$$

The linear shape functions shown in Fig. 1 are utilized, where

$$N_i^e = 1 - \eta \tag{10}$$

and

$$N_j^e = \eta, \tag{11}$$

where

$$\eta = \frac{z - z_i}{h_e} \tag{12}$$

and

$$h_e = z_j - z_i. \tag{13}$$

The matrix equation for the eth element can be written as

$$\mathbf{K}^{(e)} \cdot \Psi^{(e)} = \lambda \cdot \mathbf{M}^{(e)} \cdot \Psi^{(e)} + \mathbf{b}^{(e)} \tag{14}$$

with

$$\Psi^{(e)} = \begin{bmatrix} \psi_i \\ \psi_j \end{bmatrix}, \tag{15}$$

$$\mathbf{K}^{(e)} = \int_0^1 \begin{bmatrix} \alpha_e(\eta)/h_e + h_e\beta_e(\eta)(1-\eta)^2 & -\alpha_e(\eta)/h_e + h_e\beta_e(\eta)\eta(1-\eta) \\ -\alpha_e(\eta)/h_e + h_e\beta_e(\eta)\eta(1-\eta) & \alpha_e(\eta)/h_e + h_e\beta_e(\eta)\eta^2 \end{bmatrix} d\eta = \begin{bmatrix} K_{11}^{(e)} & K_{12}^{(e)} \\ K_{21}^{(e)} & K_{22}^{(e)} \end{bmatrix}, \tag{16}$$

$$\mathbf{M}^{(e)} = h_e \begin{bmatrix} 1/3 & 1/6 \\ 1/6 & 1/3 \end{bmatrix} = \begin{bmatrix} M_{11}^{(e)} & M_{12}^{(e)} \\ M_{21}^{(e)} & M_{22}^{(e)} \end{bmatrix}, \tag{17}$$

and

$$\mathbf{b}^{(e)} = \begin{bmatrix} \tau(z_i) \\ -\tau(z_j) \end{bmatrix}, \tag{18}$$

where ψ_i and ψ_j are the nodal values of the envelope function at z_i and z_j, respectively. $\alpha_e(\eta) = \alpha(h_e\eta + z_i)$ and $\beta_e(\eta) = \beta(h_e\eta + z_i)$. $\tau(z_i)$ and $\tau(z_j)$ are the flux terms evaluated at z_i and z_j, respectively. The flux term is given by

$$\tau(z) = -\alpha(z)\frac{d\psi(z)}{dz}. \tag{19}$$

Consider the two elements adjacent to the heterojunction at z_n as shown in Fig. 2. There are two unknowns associated with the node at z_n: ψ_n^A and ψ_n^B. There is only one unknown at a nodal point other than the heterojunction, for instance, ψ_{n-1} at z_{n-1} and ψ_n at z_n.

It follows from Eq. (14) that the element equations of the $(n-1)$th element and the nth element are

$$\mathbf{K}^{(n-1)} \cdot \Psi^{(n-1)} = \lambda \cdot \mathbf{M}^{(n-1)} \cdot \Psi^{(n-1)} + \mathbf{b}^{(n-1)} \tag{20}$$

and

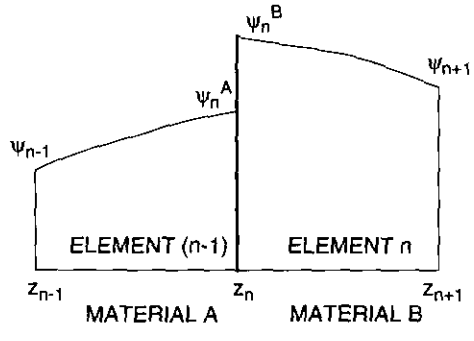

FIG. 2. The meshes adjacent to the interface. The location of the interface of materials A and B is denoted by z_n. The $(n-1)$th and the nth elements are the two meshes adjacent to the heterojunction. There are two unknowns associated with the node at z_n.

$$\mathbf{K}^{(n)} \cdot \Psi^{(n)} = \lambda \cdot \mathbf{M}^{(n)} \cdot \Psi^{(n)} + \mathbf{b}^{(n)}, \tag{21}$$

respectively, where

$$\Psi^{(n-1)} = \begin{bmatrix} \psi_{n-1} \\ \psi_n^A \end{bmatrix}, \tag{22}$$

$$\Psi^{(n)} = \begin{bmatrix} \psi_n^B \\ \psi_{n+1} \end{bmatrix}, \tag{23}$$

$$\mathbf{b}^{(n-1)} = \begin{bmatrix} \tau(z_{n-1}) \\ -\tau^A(z_n) \end{bmatrix}, \tag{24}$$

and

$$\mathbf{b}^{(n)} = \begin{bmatrix} \tau^B(z_n) \\ -\tau(z_{n+1}) \end{bmatrix}. \tag{25}$$

From Eq. (19),

$$\tau^A(z_n) = -\alpha^A(z_n)\frac{d\psi^A(z_n)}{dz} \tag{26}$$

and

$$\tau^B(z_n) = -\alpha^B(z_n)\frac{d\psi^B(z_n)}{dz}. \tag{27}$$

In addition to the four nodal unknowns (ψ_{n-1}, ψ_n^A, ψ_n^B, and ψ_n), two flux unknowns ($\tau^A(z_n)$ and $\tau^B(z_n)$) are introduced to Eqs. (20) and (21). ($\tau(z_{n-1})$ and $\tau(z_{n+1})$ are not unknowns because they will be cancelled by the flux terms of the $(n-2)$th and the $(n+1)$th elements, respectively, when the element matrices are merged.) The two flux unknowns can be eliminated by the two interface connection conditions given by Eq. (5). This paper will present two elimination methods in the next two subsections: the exact interface formulation and the finite-difference interface formulation.

2.1. *Exact Interface Formulation*

If $t_{12} \neq 0$, the interface connection conditions given by Eq. (5) can be exactly rewritten as

$$\begin{bmatrix} d\psi^A(z_n)/dz \\ d\psi^B(z_n)/dz \end{bmatrix} = \begin{bmatrix} c_{11} & c_{12} \\ c_{21} & c_{22} \end{bmatrix} \begin{bmatrix} \psi^A(z_n) \\ \psi^B(z_n) \end{bmatrix} \tag{28}$$

with

$$c_{11} = -\frac{L}{a}\cdot\frac{t_{11}}{t_{12}}, \tag{29}$$

$$c_{12} = \frac{L}{a}\cdot\frac{1}{t_{12}}, \tag{30}$$

$$c_{21} = -\frac{L}{a}\cdot\frac{\delta}{t_{12}}, \tag{31}$$

$$c_{22} = \frac{L}{a}\cdot\frac{t_{22}}{t_{12}}, \tag{32}$$

and

$$\delta = \det \tilde{\mathbf{T}}_{BA} = t_{11}t_{22} - t_{12}t_{21}. \tag{33}$$

The flux unknowns given by Eqs. (26) and (27) can be related to the nodal unknowns by Eq. (28),

$$\tau_n^A = -\alpha_n^A (c_{11}\psi_n^A + c_{12}\psi_n^B) \tag{34}$$

and

$$\tau_n^B = -\alpha_n^B (c_{21}\psi_n^A + c_{22}\psi_n^B), \tag{35}$$

where $\tau_n^A = \tau^A(z_n)$, $\tau_n^B = \tau^B(z_n)$, $\alpha_n^A = \alpha^A(z_n)$, $\alpha_n^B = \alpha^B(z_n)$, $\psi_n^A = \psi^A(z_n)$, and $\psi_n^B = \psi^B(z_n)$.

Combining Eqs. (20) and (34), the element matrix for the $(n-1)$th element becomes

$$\begin{bmatrix} K_{11}^{(n-1)} & K_{12}^{(n-1)} & 0 \\ K_{21}^{(n-1)} & K_{22}^{(n-1)} - \alpha_n^A c_{11} & -\alpha_n^A c_{12} \\ 0 & 0 & 0 \end{bmatrix} \begin{bmatrix} \psi_{n-1} \\ \psi_n^A \\ \psi_n^B \end{bmatrix} = \lambda \begin{bmatrix} M_{11}^{(n-1)} & M_{12}^{(n-1)} & 0 \\ M_{21}^{(n-1)} & M_{22}^{(n-1)} & 0 \\ 0 & 0 & 0 \end{bmatrix} \begin{bmatrix} \psi_{n-1} \\ \psi_n^A \\ \psi_n^B \end{bmatrix} + \begin{bmatrix} \tau_{n-1} \\ 0 \\ 0 \end{bmatrix}. \tag{36}$$

Similarly, the element matrix for the nth element is

$$\begin{bmatrix} 0 & 0 & 0 \\ \alpha_n^B c_{21} & K_{11}^{(n)} + \alpha_n^B c_{22} & K_{12}^{(n)} \\ 0 & K_{21}^{(n)} & K_{22}^{(n)} \end{bmatrix} \begin{bmatrix} \psi_n^A \\ \psi_n^B \\ \psi_{n+1} \end{bmatrix} = \lambda \begin{bmatrix} 0 & 0 & 0 \\ 0 & M_{11}^{(n)} & M_{12}^{(n)} \\ 0 & M_{21}^{(n)} & K_{22}^{(n)} \end{bmatrix} \begin{bmatrix} \psi_n^A \\ \psi_n^B \\ \psi_{n+1} \end{bmatrix} + \begin{bmatrix} 0 \\ 0 \\ -\tau_{n+1} \end{bmatrix}. \tag{37}$$

From Eqs. (36) and (37), the merged stiffness matrix becomes

	$n-1$	nA	nB	$n+1$
$n-1$	$K_{22}^{(n-2)} + K_{11}^{(n-1)}$	$K_{12}^{(n-1)}$	0	0
nA	$K_{21}^{(n-1)}$	$K_{22}^{(n-1)} - \alpha_n^A c_{11}$	$-\alpha_n^A c_{12}$	0
nB	0	$\alpha_n^B c_{21}$	$K_{11}^{(n)} + \alpha_n^B c_{22}$	$K_{12}^{(n)}$
$n+1$	0	0	$K_{21}^{(n)}$	$K_{22}^{(n)} + K_{11}^{(n+1)}$

(38)

where $n-1$, nA, nB, and $n+1$ represent the enumeration of the row and column of the matrix.

The merged mass matrix becomes

	$n-1$	nA	nB	$n+1$
$n-1$	$M_{22}^{(n-2)} + M_{11}^{(n-1)}$	$M_{12}^{(n-1)}$	0	0
nA	$M_{21}^{(n-1)}$	$M_{22}^{(n-1)}$	0	0
nB	0	0	$M_{11}^{(n)}$	$M_{12}^{(n)}$
$n+1$	0	0	$M_{21}^{(n)}$	$M_{22}^{(n)} + M_{11}^{(n+1)}$

(39)

Both the stiffness and the mass matrices are tridiagonal. But the stiffness matrix is not symmetric.

2.2. *Finite-Difference Interface Formulation*

The derivative term on the right-hand side of the interface connection conditions in Eq. (5) can be approximated by finite difference,

$$\frac{d\psi^A}{dz}(z_n) \approx \frac{\psi_n^A - \psi_{n-1}}{h_{n-1}}, \tag{40}$$

where $h_{n-1} = z_n - z_{n-1}$. Thus, the first interface condition can be expressed as

$$\psi_n^A \approx \frac{t_{12}(a/L)(1/h_{n-1})}{[t_{11} + t_{12}(a/L)(1/h_{n-1})]}\psi_{n-1} + \frac{1}{[t_{11} + t_{12}(a/L)(1/h_{n-1})]}\psi_n^B, \tag{41}$$

if $t_{11} + t_{12}(a/L)(1/h_{n-1}) \neq 0$. This condition of validity can always be satisfied by choosing the appropriate mesh size (h_{n-1}) of the $(n-1)$th element if $t_{11}^2 + t_{22}^2 \neq 0$.

The flux term given in Eq. (26) then becomes

$$\tau_n^A \approx \frac{\alpha_n^A t_{11}(L/a)}{[t_{11}(L/a)h_{n-1} + t_{12}]}\psi_{n-1} - \frac{\alpha_n^A (L/a)}{[t_{11}(L/a)h_{n-1} + t_{12}}\psi_n^B. \quad (42)$$

The element matrix for the $(n-1)$th element given in Eq. (20) becomes

$$\begin{bmatrix} K_{11}^{(n-1)} & K_{12}^{(n-1)} & 0 \\ K_{21}^{(n-1)} + \dfrac{\alpha_n^A(L/a)t_{11}}{[t_{11}(L/a)h_{n-1} + t_{12}]} & K_{22}^{(n-1)} & -\dfrac{\alpha_n^A(L/a)}{[t_{11}(L/a)h_{n-1} + t_{12}]} \\ 0 & 0 & 0 \end{bmatrix}$$

$$\begin{bmatrix} \psi_{n-1} \\ \psi_n^A \\ \psi_n^B \end{bmatrix} = \lambda \begin{bmatrix} M_{11}^{(n-1)} & M_{12}^{(n-1)} & 0 \\ M_{21}^{(n-1)} & M_{22}^{(n-1)} & 0 \\ 0 & 0 & 0 \end{bmatrix} \begin{bmatrix} \psi_{n-1} \\ \psi_n^A \\ \psi_n^B \end{bmatrix} + \begin{bmatrix} \tau_{n-1} \\ 0 \\ 0 \end{bmatrix}. \quad (43)$$

Using the finite difference approximation in Eq. (40), the second condition obtained from Eq. (5) can be approximated by

$$\frac{d\psi^B}{dz}(z_n) \approx t_{21}\left(\frac{L}{a}\right)\psi_n^A + t_{22}\left(\frac{\psi_n^A - \psi_{n-1}}{h_{n-1}}\right). \quad (44)$$

The flux term in Eq. (27) becomes

$$\tau_n^B \approx \left(\frac{\alpha_n^B t_{22}}{h_{n-1}}\right)\psi_{n-1} - \alpha_n^B\left[t_{21}\left(\frac{L}{a}\right) + t_{22}\left(\frac{1}{h_{n-1}}\right)\right]\psi_n^A. \quad (45)$$

From Eq. (21), the element matrix for the nth element reads

$$\begin{bmatrix} 0 & 0 & 0 & 0 \\ 0 & 0 & 0 & 0 \\ -\alpha_n^B t_{22}/h_{n-1} & \alpha_n^B[t_{21}(L/a) + t_{22}(1/h_{n-1})] & K_{11}^{(n)} & K_{21}^{(n)} \\ 0 & 0 & K_{21}^{(n)} & K_{22}^{(n)} \end{bmatrix} \begin{bmatrix} \psi_{n-1} \\ \psi_n^A \\ \psi_n^B \\ \psi_{n+1} \end{bmatrix}$$

$$= \lambda \begin{bmatrix} 0 & 0 & 0 & 0 \\ 0 & 0 & 0 & 0 \\ 0 & 0 & M_{11}^{(n)} & K_{12}^{(n)} \\ 0 & 0 & K_{21}^{(n)} & K_{22}^{(n)} \end{bmatrix} \begin{bmatrix} \psi_{n-1} \\ \psi_n^A \\ \psi_n^B \\ \psi_{n+1} \end{bmatrix} + \begin{bmatrix} 0 \\ 0 \\ 0 \\ -\tau_{n+1} \end{bmatrix}. \quad (46)$$

Merging Eqs. (43) and (46), the global stiffness matrix becomes

	$n-1$	nA	nB	$n+1$
$n-1$	$K_{22}^{(n-2)} + K_{11}^{(n-1)}$	$K_{12}^{(n-1)}$	0	0
nA	$K_{21}^{(n-1)} + \dfrac{\alpha_n^A(L/a)t_{11}}{[t_{11}(L/a)h_{n-1} + t_{12}]}$	$K_{22}^{(n-1)}$	$\dfrac{-\alpha_n^A(L/a)}{[t_{11}(L/a)h_{n-1} + t_{12}]}$	0
nB	$-\dfrac{\alpha_n^B t_{22}}{h_{n-1}}$	$\alpha_n^B\left[t_{21}\left(\dfrac{L}{a}\right) + \left(\dfrac{t_{22}}{h_{n-1}}\right)\right]$	$K_{11}^{(n)}$	$K_{12}^{(n)}$
$n+1$	0	0	$K_{21}^{(n)}$	$K_{22}^{(n)} + K_{11}^{(n+1)}$

(47)

The global mass matrix is same as the exact interface formulation given in Eq. (39).

Because of the presence of the non-vanishing matrix element at $(nB, n-1)$, the stiffness matrix is not tridiagonal.

The finite element method eventually requires the solution to a linear eigenvalue system. The Arnoldi method published by D. C. Sorensen is utilized to solve the linear eigenvalue problem with non-symmetric stiffness matrix [18].

3. RESULTS AND DISCUSSIONS

Because t_{12} of the connection matrix for the *GaAs–AlAs* interface vanishes, the finite-difference interface formulation must be used to calculate the eigenenergies of the rectangular quantum well shown in Fig. 3. The accuracy will be examined in the first subsection. In the second subsection, this numerical method will be utilized to investigate the electric field effects on the quantum well modeled by three types of *GaAs–AlAs* interface connection matrices found in the literature [5, 7, 16].

Generally, the connection matrix of the *GaAs–AlAs* interface is given by

$$\mathbf{T}(AlAs \leftarrow GaAs) = \begin{bmatrix} t_{11} & t_{12} \\ t_{21} & t_{22} \end{bmatrix}. \quad (48)$$

The matrix elements t_{11}, t_{12}, t_{21}, and t_{22} for the three types of connection matrices will be given below.

The most frequently used interface conditions are the conventional conditions of the continuity of the envelope function and the continuity of the probability flux based on the envelope function [16],

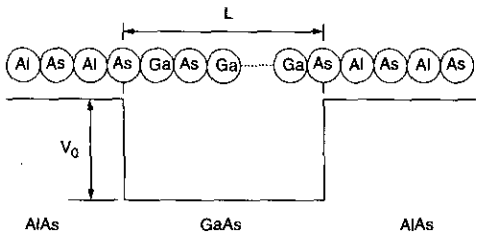

FIG. 3. The *GaAs–AlAs* quantum well. The microscopic structure and the effective-mass model of the *GaAs–AlAs* quantum well are shown in this figure.

$$t_{11} = 1, \tag{49}$$

$$t_{22} = \frac{m(AlAs)}{m(GaAs)}, \tag{50}$$

and

$$t_{12} = t_{21} = 0. \tag{51}$$

By the tight-binding model, T. Ando *et al.* deduced the effective-mass-dependent connection matrix [5],

$$t_{11} = \left[\frac{m(Al_xGa_{1-x}As)}{m(GaAs)}\frac{E_g(GaAs)}{E_g(Al_xGa_{1-x}As)}\right]^{1/2}, \tag{52}$$

$$t_{22} = \left[\frac{m(Al_xGa_{1-x}As)}{m(GaAs)}\frac{E_g(Al_xGa_{1-x}As)}{E_g(GaAs)}\right]^{1/2}, \tag{53}$$

and t_{12} and t_{21} are same as in Eq. (51).

In this paper, the band-gap energy, the effective mass, and the lattice constant of the $Al_xGa_{1-x}As$ crystal are taken to be

$$E_g(Al_xGa_{1-x}As) = \begin{cases} 1.424 + 1.247x & \text{(eV)} \\ 1.900 + 0.125x + 0.143x^2 & \text{(eV)} \end{cases}, \tag{54}$$

$$m(Al_xGa_{1-x}As) = (0.067 + 0.083x)m_0, \tag{55}$$

and

$$a(Al_xGa_{1-x}As) = 5.6533 + 0.0078x \quad (\text{Å}). \tag{56}$$

respectively [19].

From the pseudopotential model, the calculations by J. P. Cuypers *et al.* show that the connection matrix is energy-dependent and almost diagonal [7]. The matrix element t_{11} can be taken as real, and t_{22} is almost real. As the energy changes from 0 to 1.5 eV, the matrix elements t_{11} and t_{22} vary from 0.92 to 0.9 and from 1.26 to 1.05, respectively. From Fig. 3 of Ref. [7] the dependence of t_{11} and t_{22} on the energy is almost linear for energy less than 0.9 eV. Therefore, the linear relations used in this paper for $0 \le E \le 0.9$ eV are

$$t_{11} = 0.92 - \left(\frac{0.02}{1.5}\right)E, \tag{57}$$

$$t_{22} = 1.26 - \left[\frac{0.21}{1.5}\right]E, \tag{58}$$

and t_{12} and t_{21} are same as in Eq. (51), where E is the energy relative to the conduction band minimum of *GaAs*.

3.1. *Solution Accuracy*

The accuracy of the solution obtained by the finite-difference interface formulation will be studied by using the rectangular *GaAs–AlAs* quantum well with the well width of 101.7594 Å (36 monolayers of *GaAs*) and the barrier energy of 446.4 meV (assuming the band-offset ratio of 0.6) in the absence of the electric field. The finite element solutions are compared with the analytic solution obtained by the transfer matrix method [8], modified to take into account the connection matrix at the heterojunctions.

For the finite element solution, the end points of the truncated domain shown in Eq. (6) are taken to be $-x_1 = x_2 = 3$, and the number of meshes is 1900.

The eigenenergies obtained from both the analytic and the finite element methods are tabulated in Table I. The absolute and relative errors are less than 0.1 meV and 10^{-3}, respectively. Hence, the finite-difference interface formulation yields results accurate enough to explore the electric field effects.

3.2. *Electric Field Effects*

The eigenenergy dependence on the electric field predicted by the effective-mass-dependent and the energy-dependent connection matrix is compared with that predicted by the conventional interface conditions.

Under an electric field in the growth direction of the quantum well, the normalized barrier energy in Eq. (3) can be written, for a particle of charge $q = -e$, as

$$V(z) = V_0(z) + fz, \tag{59}$$

where

TABLE I

Eigenenergies of the *GaAs–AlAs* Quantum Well

Level n	E_n^{Analytic} (meV)	E_n^{FEM} (meV)	$\lvert E_n^{\text{FEM}} - E_n^{\text{Analytic}}\rvert / E_n^{\text{Analytic}}$
1	35.90507	35.87505	8.360×10^{-4}
2	141.2749	141.2141	4.305×10^{-4}
3	305.6007	305.6423	1.362×10^{-4}

Note. The rectangular *GaAs–AlAs* quantum well in the absence of the electric field is solved to study the accuracy of the solutions obtained by the finite-difference interface formulation. The eigenenergies obtained by the analytic and the finite element methods, as well as the relative errors, are tabulated.

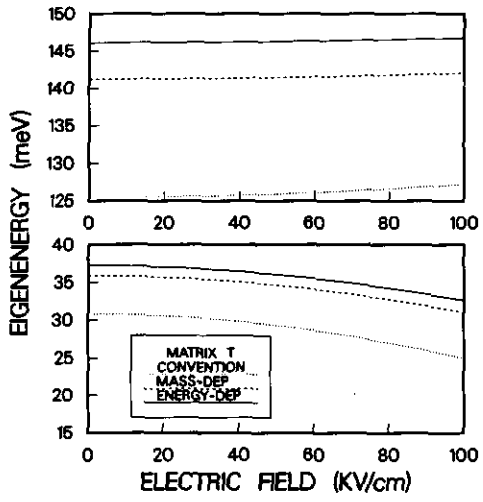

FIG. 4. Eigenenergies of the *GaAs–AlAs* quantum well. The eigenenergies of the *GaAs–AlAs* quantum well modeled by the conventional, the effective-mass-dependent, and the energy-dependent connection matrices are plotted as functions of the electric field. The lower and upper subplots represent the first and the second levels, respectively.

$$V_0(z) = \begin{cases} 1 & |z| > \frac{1}{2} \\ 0 & |z| < \frac{1}{2} \end{cases} \tag{60}$$

and

$$f = \frac{eFL}{V_0}, \tag{61}$$

where F is the physical electric field and f is the normalized field.

The quantum well with the same well width and barrier energy as in the previous subsection is solved by using the same discretization parameters. The model with the conventional interface conditions is treated as a one-domain problem because the conventional interface conditions are the natural conditions from Eq. (3) [20]. The model with the effective-mass-dependent connection matrix is solved by the multiple-domain scheme developed in Subsection 2.2. Because of the energy-dependent nature of the connection matrix, the eigenenergies of the model with the energy-dependent connection matrix are obtained by iteratively using the multiple-domain scheme to reach the self-consistent solution for each quantum level.

For the electric field varying from 0 to 100 KV/cm, the model with the conventional interface conditions predicts three quantum levels. But the third level of the models with the non-conventional matrices disappears as the field becomes greater than 50 KV/cm. Hence, for the sake of clarity in illustrations, only the eigenenergies of the first two levels are shown in Fig. 4.

In Fig. 4, the eigenenergies obtained by using the conventional, the effective-mass-dependent, and the energy-dependent connection matrices are plotted by the dotted, the dashed, and the solid curves, respectively. The lower and the upper subplots represent the first and the second levels, respectively. Of the three connection matrices, the energy-dependent connection matrix predicts the eigenenergies that are the largest in magnitude, but the least variant, as functions of the electric field. On the contrary, the conventional interface conditions predict eigenenergies that are the smallest in magnitude, but most variant, as functions of the field. It is also observed that, as the electric field increases, the first eigenenergy decreases, but the second eigenenergy increases. This behavior is similar to the infinite quantum well because the first and the second eigenenergies are far below the barrier energy [21]. Inclusion of the connection matrices at the heterojunctions does not change this qualitative trend. Moreover, Fig. 4 shows that, in comparison with the conventional connection matrix, the non-conventional connection matrices influence the second eigenenergy more than the first level.

4. CONCLUSIONS

In this paper, the irreducible finite element method is developed to incorporate the interface connection matrices at the heterojunctions of quantum wells. The interface formulation is exact only if $t_{12} \neq 0$ and can be approximated by the finite difference regardless of the value of t_{12}. For the *GaAs–AlAs* quantum well, the finite-difference interface formulation must be used, and the relative errors are less than 10^{-3}.

This finite element method is applied to compare the electric field effects on the *GaAs–AlAs* quantum well modeled by the conventional, the effective-mass-dependent, and the energy-dependent connection matrices. The energy-dependent connection matrix predicts the largest eigenenergies and the conventional connection matrix predicts the smallest eigenenergies. In comparison with the conventional connection matrix, the non-conventional connection matrices elevate the eigenenergies of the excited levels more than the eigenenergy of the first level, and the eigenenergies predicted by the non-conventional model are less field-dependent.

ACKNOWLEDGMENTS

The authors would like to express sincere gratitude to Dr. D. C. Sorensen for providing us with the source codes for the linear eigensolver employing the Arnoldi method. We also thank Drs. M. Luke and K. Nakamura for their comments. This work is supported by the U.S. National Science Foundation under Grant No. ECS-9158036.

REFERENCES

1. J. M. Luttinger and W. Kohn, *Phys. Rev.* 97(4), 869 (1955).
2. T. Ando and S. Mori, *Surf. Sci.* **113,** 124 (1982).
3. H. Akera, S. Wakahara, and T. Ando, *Surf. Sci.* **196,** 694 (1988).
4. A. Ishibashi, Y. Mori, K. Kaneko, and N. Watanabe, *J. Appl. Phys.* **59**(12), 4087 (1986).
5. T. Ando, S. Wakahara, and H. Akera, *Phys. Rev. B* **40**(17), 11609 (1989).

6. T. Ando and H. Akera, *Phys. Rev. B* **40**(17), 11619 (1989).
7. J. P. Cuypers and W. van Haeringen, *Phys. Rev. B* **47**(16), 10310 (1993).
8. E. Merzbacher, *Quantum Mechanics*, 2nd ed. (Wiley, New York, 1970)
9. K. Nakamura, A. Shimizu, M. Koshiba, and K. Hayata, *Electron. Commun. Japan Part 2* **72**(9), 29 (1989).
10. K. Nakamura, A. Shimizu, M. Koshiba, and K. Hayata, *IEEE J. Quantum Electron.* **25**(5), 889 (1989).
11. K. Nakamura, A. Shimizu, K. Koshiba, and K. Hayata, *Electron. Commun. Japan Part 2* **73**(12), 1 (1990).
12. K. Nakamura, A. Shimizu, M. Koshiba, and K. Hayata, *IEEE J. Quantum Electron.* **27**(8), 2035 (1991).
13. K. Nakamura, A. Shimizu, K. Fujii, M. Koshiba, and K. Hayata, *IEEE J. Quantum Electron.* **28**(7), 1670 (1992).
14. K. Nakamura, A. Shimizu, M. Koshiba, and K. Hayata, *IEEE J. Quantum Electron.* **27**(5), 1189 (1991).
15. O. C. Zienkiewicz and K. Morgan, *The Finite Element Method, Vol.* 1, 4th ed. (McGraw-Hill London, 1989).
16. D. J. BenDaniel and C. B. Duke, *Phys. Rev.* **152**(2), 683 (1966).
17. M. G. Burt, *Semicond. Sci. Technol.* **3,** 739 (1988).
18. D. C. Sorensen, *SIAM J. Matrix Anal. Appl.* **13**(1), 357 (1992).
19. S. Adachi, *J. Appl. Phys.* **58**(3), R1 (1985).
20. T. L. Li and K. J. Kuhn, *J. Comput. Phys.* **110**(2), 292 (1994).
21. T. Hiroshima and R. Lang, *Appl. Phys. Lett.* **49** (11), (1986).